EXPLORING ARYL-SUBSTITUTED 1,2,3-TRIAZOLES: SYNTHESIS, CHARACTERIZATION, AND THEORETICAL INVESTIGATIONS

CRISTIAN VALDEBENITO [a], DAVID MORENO DA COSTA [b], JOSÉ GAETE [c,d], ALEJANDRO TORO-LABBÉ [e], KARINA MUÑOZ-BECERRA [a], GABRIEL ABARCA[f*] AND CESAR MORALES-VERDEJO [g*]*

[a]*Universidad Bernardo O'Higgins, Facultad de Ciencias de la Salud, Centro Integrativo de Biología y Química Aplicada (CIBQA), General Gana 1702, Santiago, Chile.*

[b] *Universidad Bernardo O'Higgins, Centro de Investigación en Ciberseguridad (CICS), Avenida Viel 1497, Santiago, Chile.*

[c] *Universidad Bernardo O'Higgins, Facultad de Ingeniería, Ciencia y Tecnología, Escuela de Ingeniería civil y Ciencias Geoespaciales, Av. Viel 1497, Santiago, Chile.*

[d] *Universidad Bernardo O´Higgins, Facultad de Ingeniería, Ciencia y Tecnología, Centro de Investigación de Desastres y Gestión Sostenible de Recursos, Av. Viel 1497, Santiago, Chile.*

[e] *Facultad de Química y de Farmacia, Pontificia Universidad Católica de Chile, Santiago, Chile.*

[f] *Universidad Bernardo O´Higgins, Vicerrectoría Vinculación con el Medio, Dirección General de Vinculación con el Medio, General Gana 1702, Santiago, Chile.*

g *Universidad Bernardo O´Higgins, Vicerrectoría Académica, Dirección General de Investigación, Innovación, Transferencia y Emprendimiento, General Gana 1670, Santiago, Chile.*

ABSTRACT

This study synthesized newly designed 1,2,3-triazoles substituted with aryl groups via Sharpless' copper(I)-catalyzed azide-alkyne cycloaddition. The resulting compounds were extensively characterized using NMR and UV-Vis spectroscopy. Furthermore, theoretical DFT and time-dependent DFT calculations were performed to analyze the structural and electronic properties of these molecules. Computational analysis revealed insights into the electron distribution within these molecules, with the electron-withdrawing or electron-donating nature of the substituents affecting the HOMO-LUMO gap. These findings provide valuable information for tailoring the electronic properties of triazole-containing compounds, making them suitable for various chemical applications and potential coordination with metalloporphyrins.

Keywords: 1,2,3-triazoles disubstituted, copper(I)-catalyzed, azide-alkyne cycloaddition, DFT calculations.

INTRODUCTION

The synthesis of triazoles from alkynes has emerged as a pivotal and valuable methodology for crafting diverse molecules with multifunctional attributes. By modifying alkynes and nitrogen sources such as azides, various analogs of 1,4-disubstituted triazoles have been successfully obtained for various applications.[1,2] The enhancement of triazole synthesis has been achieved by employing copper catalysts to selectively generate one of the two isomers produced under thermal conditions, enabling the creation of specific compound families.[3] Moreover, significant contributions to this field have arisen from the development of synthetic methods employing various transition metals including gold, iridium, iron, nickel, ruthenium, samarium, silver, and zinc, facilitating the cyclization of alkynes and nitrogen sources.[4]

Additionally, there has been a growing interest in recent years in devising straightforward, environmentally friendly, cost-effective, and non-toxic protocols. In this regard, the reaction of alkynes with nitrogen sources, conducted entirely without the involvement of transition metals, satisfies many of these criteria, offering an excellent alternative for triazole synthesis.

Among N-heterocycles, triazoles and their substituted derivatives have garnered significant attention for various purposes due to their intriguing properties and potential applications in therapeutic biology. These include antiproliferative 1,2,4-triazole analogs akin to combretastatin, anticonvulsant phenacyl triazole hydrazones,[5,6] antimicrobial thioethereal 1,4-disubstituted 1,2,3-triazole esters,[7] antineoplastic 1,2,3-triazole-4,5-*bis*(isopropyl carbamate) glucopyranosides,[8] antiviral □-arylalkyl-1*H*-1,2,4-triazoles,[9] analgesic thiazolo[3,2-*b*]-1,2,4-triazoles derived from naproxen,[10] anti-inflammatory oxazolo[4,5-*b*]pyridine-2-one 1,2,3-triazoles,[11] anticancer quinazolin-4(3*H*)-one 1,2,3-triazole analogues,[12] antimalarial 1,2,4-triazole analogues.[13] Additionally, many heterocycles incorporating a triazole scaffold within their structures exhibit distinctive structural and electronic properties [14] and are utilized in organic synthesis for pioneering reactions.[15,16]

The copper(I)-catalyzed azide-alkyne cycloaddition, widely explored in previous studies, has been employed to synthesize 1,2,3-triazoles, [17,18] which have found applications in the development of metal complexes and potential biological uses.[3] Typically, methodologies involving the use of copper(I) ligands are introduced to form an in-situ copper(I) complex species within the reaction medium, ensuring the stabilization of Cu(I). Alternatively, Cu(II) can also be utilized by adding a reductive agent, such as sodium ascorbate. [3]

Our research delves into the synthesis of diaryl-substituted triazoles featuring methylthio groups, enabling their attachment to metal surfaces for various chemical and technological applications. Inspired by the work of Pizarro et al.,[19] which demonstrated that non-condensed polycyclic heteroaromatic hydrocarbons with sulfur groups in an axial position can be linked to gold surfaces for use in oxygen reduction reactions. These systems, referred to as molecular wires, can be coordinated with metalloporphyrins, characterized by an iron(II) core, for the electrocatalytic reduction of molecular oxygen.

To explore the capacity of different heteroaromatic hydrocarbons, we concentrated our efforts on synthesizing 1,2,3-triazoles that are 1,4-disubstituted, bearing the necessary methylthio and pyridine groups. The former facilitates attachment to the gold surface, while the latter allows for coordination with the iron core in metalloporphyrins, as previously reported by Zagal.[19] In this article, we present the results of synthesizing non-condensed polycyclic heteroaromatic hydrocarbons featuring the 1,2,3-triazole moiety.

2. MATERIALS AND METHODS

2.1. General information

The starting materials 4-Bromothioanisole, trimethylsilylacetylene, 4-Aminophenol, 4-iodoaniline, and 4-Aminopyridine were purchased from Merck-Sigma Aldrich. The synthesis of 4-(pyridin-4-yl)aniline and (4-ethynyl phenyl)(methyl)sulfane has been reported previously.[20,21] The solvents were purchased from Merck-Millipore. The NMR characterization was achieved by Bruker AVANCE 400 spectrometer. The infrared spectra were collected in a JASCO 4100 Fourier transform infrared spectrometer. The UV-Vis spectroscopy was performed in a JASCO V-630 spectrophotometer, and samples were contained on 1 cm path-length quartz cuvettes.

2.2. General procedure for the organic azides

In the first step, the amine derivative precursors such as 4-aminophenol, 4-iodoaniline, 4-aminopyridine, and 4-(pyridin-4-yl)aniline (3.6 mmol) were dissolved in HCl 1.5 M solution. Then, $NaNO_2$ (3.6 mmol) was added at 0 °C, and the reaction was kept under stirring for 1 h. In a second step, NaN_3 (3.8 mmol) was added, and the reaction was kept under stirring for 1 additional hour. Finally, the reaction mixture was poured into ice water, and the product was extracted with dichloromethane. The compounds were not purified and were immediately used to synthesize the respective triazoles.

*Corresponding author email: karina.muñoz@ubo.cl, gabriel.abarca@ubo.cl, cesar.morales@ubo.cl

2.3. General procedure for the triazoles

2.3.1 4-(4-(4-(methylthio)phenyl)-1*H*-1,2,3-triazol-1-yl)phenol (1)

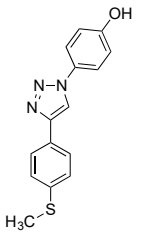

(4-ethynyl phenyl)(methyl)sulfane (1.65 g, 11.10 mmol, 1.0 eq.), 4-aminophenol derivative azide (1.50 g, 11.10 mmol, 1.0 eq.), $CuSO_4 \cdot 5H_2O$ (177.4 mg, 0.71 mmol, 0.064 eq.), and sodium ascorbate (879.7 mg, 4.44 mmol, 0.4 eq) were loaded into a 50 mL round-bottom tube flask and dissolved in a mixed solvent DMF/H_2O (4:1). The reaction was stirred for 48 h at room temperature. After its completion, the water-insoluble triazole **1** was recovered by filtration as a brownish powder and washed with water to give a brown solid with an 87% yield.

UV−vis (DMSO), λ_{max}, 286 nm

^{1}H NMR (400 MHz, DMSO-d_6) δ 8.73 (s, 1H), 7.83 (d, *J* = 8.1 Hz, 2H), 7.64 (d, *J* = 8.5 Hz, 2H), 7.38 (t, *J* = 5.5 Hz, 2H), 6.96 (d, *J* = 8.5 Hz, 2H), 2.90 (s, OH), 2.48 (s, 3H).

^{13}C NMR (101 MHz, DMSO) δ 157.28, 137.47, 128.54, 127.10, 126.67, 125.43, 121.40, 118.56, 115.61, 39.52, 14.80.

DEPT NMR (101 MHz, DMSO) δ 126.68, 125.43, 121.40, 118.57, 115.62, 14.80.

FT-IR (cm^{-1}, KBr) 3387 (**s**), 3067 (**w**), 2919 (**w**), 2591 (**w**), 1652 (**s**), 1605 (**s**), 1536 (**s**), 1519 (**s**), 1480 (**s**), 1434 (**s**), 1407 (**m**), 1382 (**m**), 1353 (**m**), 1229 (**s**), 1168 (**m**), 1087 (**s**), 1058 (**s**), 967 (**s**), 892 (**w**), 836 (**s**), 809 (**s**), 720 (**w**), 628 (**m**), 518 (**s**).

2.3.2 1-(4-iodophenyl)-4-(4-(methylthio)phenyl)-1*H*-1,2,3-triazole (2)

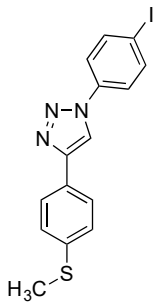

(4-ethynyl phenyl)(methyl)sulfane (5.0 mmol, 1.0 eq.), 4-iodoaniline derivative azide (1.0 eq.), $CuSO_4 \cdot 5H_2O$ (0.1 eq.), and sodium ascorbate (0.4 eq) were loaded into a 25 mL round-bottom flask and dissolved in a mixed solvent DMF/H_2O (4:1). The reaction was stirred for 48 h at room temperature. After its completion, the water-insoluble triazole **2** was recovered by filtration as a grey powder with a 93% yield.

UV−vis (DMSO), λ_{max}, 287 nm

^{1}H NMR (400 MHz, DMSO-d_6) δ 8.68 (d, *J* = 0.8 Hz, 1H), 7.68 (d, *J* = 8.7 Hz, 2H), 7.58 (d, *J* = 8.4 Hz, 2H), 7.45 (d, *J* = 8.8 Hz, 2H), 7.13 (d, *J* = 8.4 Hz, 2H), 2.25 (s, 3H).

^{13}C NMR (101 MHz, DMSO) δ 146.58, 137.90, 137.77, 126.62, 125.43, 121.53, 121.50, 118.41, 118.38, 92.52, 39.52, 14.71.

DEPT NMR (101 MHz, DMSO) δ 137.93, 126.62, 125.44, 121.54, 118.43, 14.71.

FT-IR (cm^{-1}, KBr) 3442 (**w**), 3355 (**w**), 3209 (**w**), 3118 (**s**), 3091 (**s**), 2973 (**w**), 2912 (**w**), 1911 (**w**), 1652 (**w**), 1606 (**w**) 1586 (**w**), 1549 (**w**), 1481 (**s**), 1480 (**s**), 1432 (**s**), 1398 (**s**), 1338 (**w**), 1308 (**w**), 1280 (**w**), 1239 (**s**), 1227 (**s**), 1179 (**w**), 1105 (**s**), 1082 (**s**), 1039 (**s**), 1011 (**m**), 989 (**s**), 826 (**s**), 818 (**s**), 813 (**s**) 725 (**m**), 697 (**w**), 519 (**s**), 515 (**s**), 469 (**s**).

2.3.3 4-(4-(4-(methylthio)phenyl)-1*H*-1,2,3-triazol-1-yl)pyridine (3)

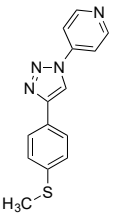

(4-ethynyl phenyl)(methyl)sulfane (1.65 g, 11.10 mmol, 1.0 eq.), 4-Aminopyridine derivative azide (1.33 g, 11.10 mmol, 1.0 eq.), $CuSO_4 \cdot 5H_2O$ (177.4 mg, 710.4 mmol, 0.06 eq.), and sodium ascorbate (879.6 mg, 4.44 mmol, 0.4 eq.) were loaded into a 25 mL round-bottom tube flask and dissolved in a mixed solvent DMF/H_2O (4:1). The reaction was stirred for 48 h at room temperature. After its completion, the water-insoluble triazole **3** was recovered by filtration as a brownish powder (77%).

UV−vis (DMSO), λ_{max}, 290 nm

1H NMR (400 MHz, DMSO-d6) δ 8.95 (s, 1H), 7.94 (d, *J* = 7.7 Hz, 2H), 7.82 (d, *J* = 9.2 Hz, 2H), 7.69 (d, *J* = 6.1 Hz, 2H), 7.37 (d, *J* = 7.6 Hz, 2H), 2.73 (s, 3H).

^{13}C NMR (101 MHz, DMSO) δ 153.65, 146.53, 137.86, 137.73, 131.89, 131.73, 130.97, 130.83, 126.59, 125.38, 121.47, 119.62, 118.37, 39.52, 14.69.

DEPT NMR (101 MHz, DMSO) δ 137.86, 131.89, 130.97, 126.60, 125.88, 125.39, 121.47, 119.62, 118.37, 14.69.

FT-IR (cm^{-1}, KBr) 3136 (**w**), 2912, (**w**) 1585(**w**), 1497 (**w**), 1481 (**w**), 1431 (**w**), 1396 (**w**), 1227 (**w**), 1093 (**w**), 1082 (**w**), 989 (**w**), 812 (**s**).

2.3.4 4-(4-(4-(methylthio)phenyl)-1*H*-1,2,3-triazol-1-yl)phenyl)pyridine (4)

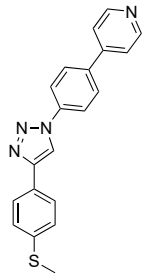

(4-ethynyl phenyl)(methyl)sulfane (377.7 mg, 2.55 mmol, 1.0 eq.), respective azide pyridyl phenyl azide (500 mg, 2.55 mmol, 1.0 eq.), $CuSO_4 \cdot 5H_2O$ (40.75 mg, 163.2 mmol, 0.06 eq.), and sodium ascorbate (202.1 mg, 1.02 mmol, 0.4 eq) were loaded into a 25 mL round-bottom tube flask and dissolved in a mixed solvent DMF/H_2O (4:1). The reaction was stirred for 48 h at room temperature. After its completion, the water-insoluble triazole **4** was recovered by filtration as a yellowish powder (90%).

UV−vis (DMSO), λ_{max}, 291 nm

^{1}H NMR (400 MHz, DMSO-d_6) δ 8.95 (s, 1H), 7.93 (d, *J* = 8.9, 4H), 7.84 (d, *J* = 8.2, 4H), 7.70 (d, *J* = 8.9 Hz, 4H), 7.40 (d, *J* = 8.4 Hz, 2H), 2.44 (s, 3H).

^{13}C NMR (101 MHz, DMSO) δ 133.7, 127.5, 126.6, 125.4, 120.1, 118.5, 39.5, 14.7.

^{13}C NMR-DEPT (101 MHz, DMSO) δ 135.1, 128.7, 127.9, 126.7, 121.4, 119.7.

FT-IR (cm^{-1}, KBr) 3121 (**m**), 3047 (**w**), 2915 (**w**), 1606 (**s**), 1548 (**m**), 1528 (**m**), 1482 (**s**), 1433 (**s**), 1401 (**s**), 1340 (**w**), 1226 (**s**), 1154 (**w**), 1120 (**w**), 1104 (**s**), 1083 (**m**), 1041 (**s**), 1014 (**m**), 991 (**s**), 811 (**s**), 744 (**w**), 720 (**w**), 694 (**s**), 524 (m), 510 (**s**).

2.4 Computational details.

The optimization of the molecular structures of compounds **1** – **4** at their energy minimum was performed at the density functional theory (DFT) in the Gaussian 16 software.[22] The B3LYP/6-311+g(d,p) [23–26] level of theory was applied in the gas phase and included DMSO as a solvent, using the solvation model based on the molecular electron density (SMD).[27] Iodine in compound **2**

was described with the LANL2DZ pseudopotential.[28] The solvent was also included in the study of the UV-Vis properties using the time-dependent DFT method under the same theoretical framework. The UV–vis absorption spectra were calculated using the 50 lowest singlet-singlet excitation states. The theory level was chosen considering previous works on electronic and photophysical properties of 1,2,3-triazole.[29–36] In all calculations, the DFT-GD3BJ dispersion correction was considered to include dispersion force effects on the energy.[37] The analytical frequency calculations confirmed the energy minimum of the optimized structures. The wavefunction analyses as the topological analyses were performed in the Multiwfn program.[38]

3. RESULTS AND DISCUSSION

3.1. SYNTHESIS AND CHARACTERIZATION

3.1.1 Synthesis of the 4-(4-(4-(4-(methylthio)phenyl)-1H-1,2,3-triazol-1-yl)phenyl)pyridine analogues

The synthesis 4-(4-(4-(4-(methylthio)phenyl)-1H-1,2,3-triazol-1-yl)phenyl)pyridine analogs start by preparing the azide derivative from the precursors 4-aminophenol, 4-iodoaniline, 4-aminopyridine, and 4-(pyridin-4-yl)aniline in an acid solution and $NaNO_2$ at low temperature (0 ºC), followed by the addition of NaN_3, obtaining the respective azide derivative with a yield of over 75%. (Scheme 1)

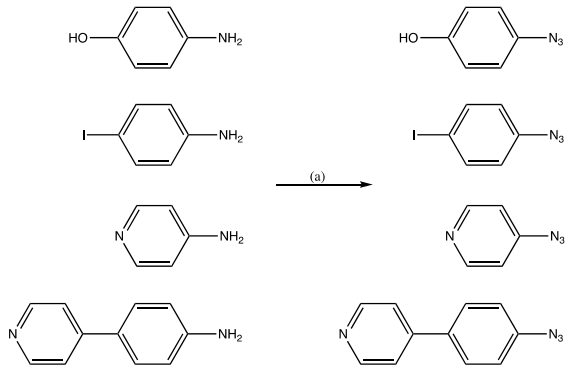

Scheme 1: General procedure for the organic azide precursors. (a) (i) HCl (1.5M), $NaNO_2$, (ii) NaN_3, 0 ºC, 1 h.

Compounds **1**-**4** were synthesized under click reaction conditions by reacting one equivalent of azide precursors with one equivalent of (4-ethynylphenyl)(methyl)sulfane as described in Scheme 2, obtaining a yield over 77%. All compounds obtained have low solubility in commonly used organic solvents.

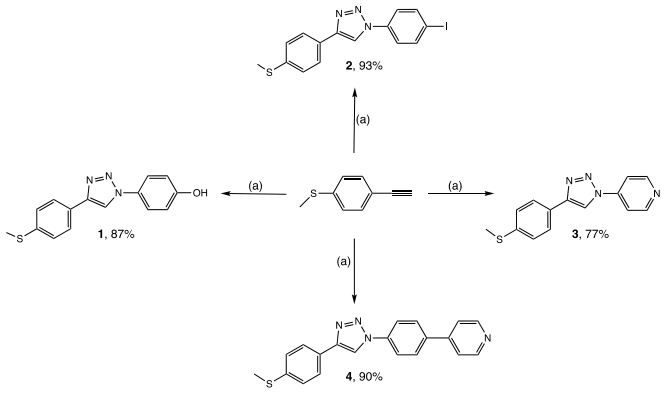

Scheme 2. Reagents and conditions: (a) respective Aryl azide, $CuSO_4{\cdot}5H_2O$, sodium ascorbate, DMF/H_2O, 48 h.

3.1.2 NMR and FT-IR characterization of the ligands

All compounds were characterized by ^1H, ^{13}C NMR, and FT-IR. For the NMR analysis, the samples were prepared in DMSO-d_6, and the spectra were collected at 140º C due to the poor solubility of the triazoles. No signals were identifiable when the spectra were measured at room temperature because the triazoles were insoluble. On the other hand, when the spectra were collected at 140º C, consistent signals were appreciated, and, in all cases, the number of signals was coherent with the molecular structures.

According to the data, all compounds **1** to **4** exhibit distinctive signals patrons compose for three zones in the ^1H NMR spectra. The first zone corresponds to the hydrogen in the triazole core, which exhibits shifts in the range of 8.95 to 8.68 ppm (Fig.1, Fig.S1, Fig.S3, and Fig.S6). Compounds **1** and **2** show a discrete difference in the chemical shifts: 8.74 and 8.68 ppm. In contrast to the same proton signal in **3** and **4**, the hydrogen in these triazole cores is less shielded than in **1** and **2**, with a chemical shift of 8.95 ppm.

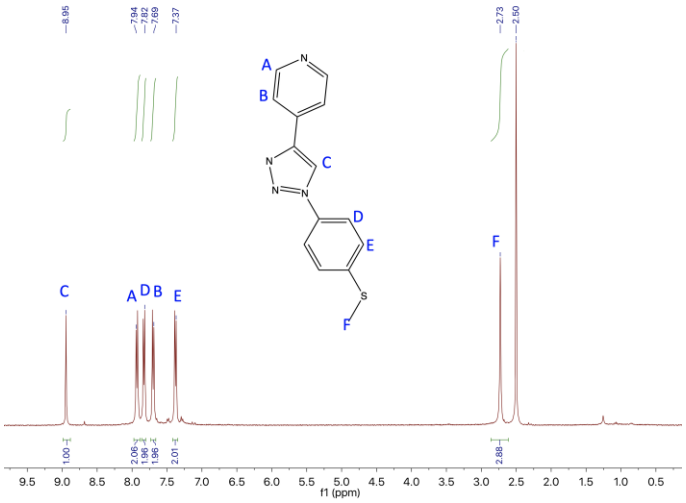

Figure 1. ^1H-NMR spectrum of 4-(4-(4-(methylthio)phenyl)-1H-1,2,3-triazol-1-yl)pyridine **(3)** in DMSO-d_6**.**

The second zone corresponds to aromatic signals of the benzyl and pyridine groups, which exhibit shifts in the 7.94 to 6.95 ppm range. These four patterns are present in all proton NMR reported.

The third zone corresponds to the methyl group signal, which exhibits shifts in the 2.73 to 2.25 ppm range. In the same way as the triazole proton, an effect on the pair of compounds **1** and **2** versus compounds **3** and **4** was observed, obtaining less shielded hydrogens for **3** – **4** compared to **1** – **2**.

Regarding compound **1**, the signal of OH appears at 2.90 ppm, which means that the local magnetic field experienced by the proton is weaker, leading to a higher resonance frequency or a high-field shift. It is known that, in the case of the OH (hydroxyl) group, the chemical environment around the proton can have different effects depending on the specific molecule. In some cases, the OH group can exhibit a high-field signal; in others, it can display a low-field signal. The specific chemical shift of the OH group will depend on factors such as the electronic environment, neighboring atoms, and molecular structure. In our case, it is suggested that the chemical environment adjacent to the OH group with the triazole group leads to a relatively high-field signal.

The most notable signal in the ^{13}C NMR spectra in the 14.68 to 14.80 ppm range corresponds to the carbons of the methyl group for each species reported here. On the other hand, compound **2** showed a signal at 92.52 ppm attributed to the quaternary carbon attached to the iodine atom (Fig. 4).

Concerning FT-IR studies, all the compounds here reported present absorption bands in the regions 3080-3100, 1549- 1606, and 1319-1340 cm^{-1} indicate a five-membered triazole ring for the stretching of C-H, C-N, and N=N respectively (Fig. 2 and Fig. S8 - S10).[39] Table 1 summarizes the reported main stretching frequencies for compounds **1** – **4**. Compound **1** shows a clear stretching band corresponding to the O-H group of its chemical structure at 3387 cm^{-1} (Fig. 2).

For all compounds, the peak at 2916 cm^{-1} is assigned to C-H stretching vibrations of the methylthio group. The peak at 1483 cm^{-1} is assigned to C=C stretching vibrations of the aromatic fragment.

Table 1. Main Stretching Frequencies of FT-IR spectra.

Compound	Wavenumber (cm^{-1})	Vibration type	Assignment
1	722	Stretching	C-S
	1483	Stretching	C=C (aromatic)
	2916	Stretching	C-H
	1318	Stretching	C-N
	1549	Stretching	N=N
	3149-3493	Stretching	O-H
2	724	Stretching	C-S
	1480	Stretching	C=C (aromatic)
	2912	Stretching	C-H
	1318	Stretching	C-N
	1548	Stretching	N=N
3	724	Stretching	C-S
	1481	Stretching	C=C (aromatic)
	2912	Stretching	C-H
	1319	Stretching	C-N
	1549	Stretching	N=N
4	720	Stretching	C-S
	1482	Stretching	C=C (aromatic)
	2915	Stretching	C-H
	1340	Stretching	C-N
	1606	Stretching	N=N

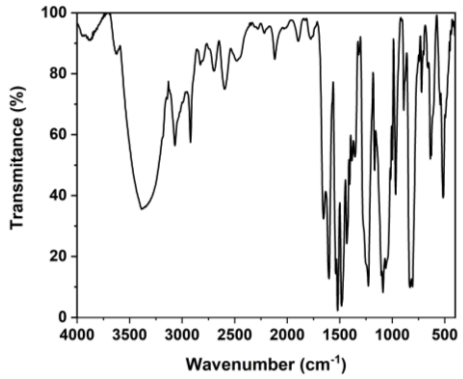

Figure 2. FT-IR spectrum of 4-(4-(4-(methylthio)phenyl)-1H-1,2,3-triazol-1-yl)phenol **(1)**.

3.1.3 UV-visible spectroscopy and computational analysis.

The 1,2,3-triazoles 1,4-disubstituted were experimentally designed to include a methylthio-phenyl able to link the molecules over conductive surfaces as gold. On the other hand, the R-substituents modulate the charge transfer properties of the molecules and explore the diversity of the designed molecules as possible axial ligands for coordination compounds such as metalloporphyrins.[19] In this way, the synthesized molecules **1** – **4** have a common structural pattern consisting of a methylthio-phenyl unit connected to a C(4)-substituted 1,2,3-triazole moiety. Phenol, iodophenyl, pyridine, and phenyl pyridine are N(1) substituents in molecules **1**, **2**, **3**, and **4**, respectively, as depicted in Figure 3.

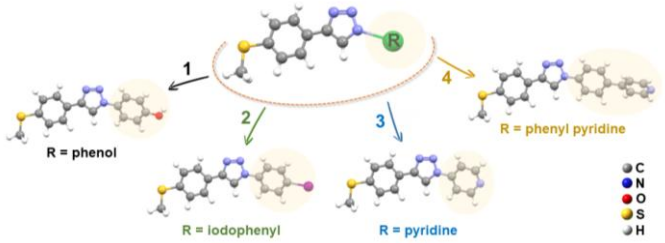

Figure 3. Structures of compounds **1** – **4**, showing the common structural pattern of methylthio-phenyl and 1,2,3-triazole, and the corresponding R-substituents.

Figure 4 shows the UV-Vis spectra obtained for compounds **1** – **4** in DMSO. An intense λ_{max} band for **1**, **2**, **3,** and **4** appears at 286.4 nm (Abs. 0.855), 287 nm (Abs. 0.743), 290.6 nm (Abs. 0.367) and 290.2 nm (Abs. 0.812), respectively. In addition, for compounds **3** and **4**, a shoulder is observed at a higher wavelength than the λ_{max} band (a redshifted shoulder at 323 and 331 nm, respectively), also observed in previously reported triazole derivatives compounds.[30,36,40–44] To explain the electronic properties of these compounds as the observed λ_{max} tendency (Fig. 4), we studied their electronic structure by geometry optimization through DFT in DMSO solvent. The theoretical UV-Vis spectra were obtained using the TD-DFT method (see Computational Details).

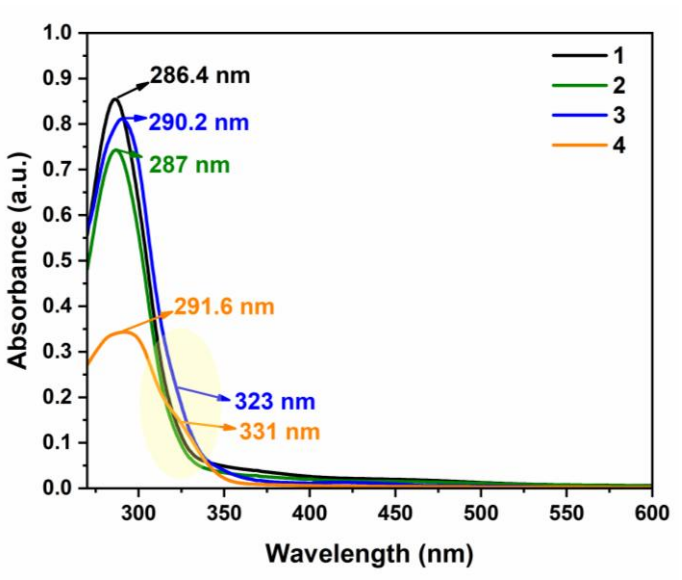

Figure 4. The UV-Vis absorption spectrum of compounds **1** – **4**.

The effect of the R-substituent in the electronic behavior of the molecules is related to their ability to withdraw or donate electrons from the structure, influencing their UV-Vis in terms of wavelength and adsorption intensity.[41] Figure 5 shows the energy and electron density distribution of the highest-occupied molecular orbital (HOMO) and the lowest-unoccupied molecular orbital (LUMO) for **1** – **4**. Each structure's π-bonding type HOMO is mainly localized over the common methylthio-phenyl-C(4)-1,2,3-triazole unit, while the LUMO, with a π-bonding type, is mainly confined over the corresponding R-substituent and N(1)-1,2,3-triazole moiety, with almost no contribution over the methylthio group (except for **1** that shows a little contribution over the S atom). Figure 5 shows that the electron-donating character of -OH in **1** destabilized the LUMO (relative to the rest of the series), shifting its electron distribution involving the S atom of the methyl-thio group. Conversely, the electron-withdrawing character of the iodophenyl, pyridine, and phenyl-pyridine units in **2**, **3,** and **4** stabilized the LUMO among the series. The LUMO energy trend follows **1** > **2** > **3** = **4**, reflecting the moderately electron-withdrawing nature of iodophenyl in **2**. Due to its ability to share π-electron pairs in aromatic rings, iodine's electron-withdrawing character, which is related to its considerable electronegativity, is surpassed. This is related to its high ionic radius and soft-base character and explains the poor contribution of I to the LUMO as its lower relative stability compared to **3** and **4** (Fig. 5). For the above, pyridine and phenyl-pyridine N(1)-substituents induce a high LUMO stability due to their electron-withdrawing character. The lower contribution of the methylthio-phenyl unit in the LUMO of **4** results from the phenyl-pyridine moiety. This has an additional aromatic ring than the pyridine substituent in **3**, which is expected to increase the pyridine's electron-withdrawing character. The calculated HOMO-LUMO gap (Fig. 5, Fig. S13) follows the tendency **1** > **2** > **3** > **4**, thus being related to the electronic nature of the R-substituent as the electron-withdrawing character of the R-substituent increases the H-L gap decreases.

Table 2. Experimental and theoretical parameters for the UV-Vis excitations for the synthesized compounds. The computed excitations with the highest oscillator strength in each case were included in the analysis.

Compound	$\lambda_{exp\text{-}max}$ (nm)	$\lambda_{exp\text{-}shoulder}$ (nm)	λ_{theo} (nm)	*f*	Orbitals	Transition character
1	286.4	---	311.8	0.367	H → L (96%)	π → π / n → π
			289.8	0.640	H → L+1 (91%)	π → π* / n → π*
2	287	---	330.4	0.257	H → L (98%)	π → π / n → π
			293.7	0.572	H → L+1 (68%)	π → π* / n → π
					H → L+2 (24%)	π → π* / n → π
3	290.2	323	358.4	0.157	H → L (99%)	π → π / n → π
			294.7	0.658	H → L+1 (97%)	π → π* / n → π
4	291.6	331	356.1	0.225	H → L (98%)	π → π / n → π
			295.8	0.943	H → L+1 (85%)	π → π* / n → π
					H-1 → L (9%)	π → π / n → π

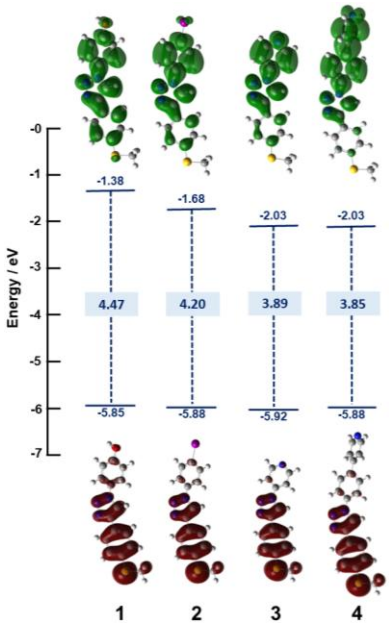

Figure 5. Representation of the HOMO (E_{HOMO}), LUMO (E_{LUMO}), and H-L gap energies (eV) for the synthesized compounds **1** – **4**, showing the corresponding HOMO and LUMO density surfaces (isovalue = 0.004 a.u).

Figure 6a shows the linear tendency obtained between the calculated H-L gap for **1** – **4** as a function of their experimental λ_{max} (Fig. 4, Table 2). This trend indicates that the λ_{max} redshift observed for **3** and **4** results from the electronic effect of the pyridine and phenyl-pyridine moieties, respectively. In addition, they should be responsible for the observed shoulder in **3** and **4** (323 nm and 331 nm, respectively; Fig. 4). Figure 6b depicts the correlation between the experimental and theoretical λ_{max} values for **1** – **4**. The TD-DFT calculations were carried out with three theory levels (Fig. S11 and S12), with the B3LYP/6-311+g(d,p) being the most accurate in terms of the studied UV-Vis experimental-theoretical correlations. The theoretical λ_{max} values correspond to the computed electronic transition having the highest oscillator strength (*f*). The electronic transitions in **1** – **4** mainly involve electron transfer from HOMO to LUMO and LUMO+1 (Fig. S13, Table 2), in concordance with previous studies for triazole derivative species.[29–31,33,34,36,40] These H→L and H→L+1 electron transfers are related to π → π and π → π* transitions, respectively, with charge transfer (CT) character. Since the HOMO has a contribution of p orbitals of S atom (Fig. 5), n → π and n → π* transitions are also involved in these electron transfers. In the case of **3** and **4**, the observed shoulders are related to the redshift of the HOMO-LUMO transitions as a product of the influence of corresponding pyridine and phenyl-pyridine substituents. In contrast, these shoulders have higher energies for **1** and **2**, thus being contained within the experimental λ_{max} transition. The redshift of the adsorption bands due to electron-withdrawing substituents over triazole-derivatives has been observed in previous studies.[34,40,41]

It is well known that the π-conjugation degree is a critical factor in CT processes. The planarity lost in a molecular structure can be detrimental for CT since it limits the π-π electronic conjugation among sp^2 units.[41,45] Figure 6c shows the dihedral N2-N3-C-C angle measured between the triazole and phenyl ring planes (Fig. S14). It is observed that higher dihedral angles for **1** and **2** correlate with lower λ_{max}, while more planar molecule **3** correlates with higher λ_{max}. Nevertheless, the linearity of this trend is lost when considering the dihedral angle of **4**. Molecule **4** contains an extra phenyl ring compared to molecule **3,** which contributes to electronic conjugation through the molecule. This is consistent with previous research on the optical properties of derivatives containing 1,2,3-triazole.[41,45]

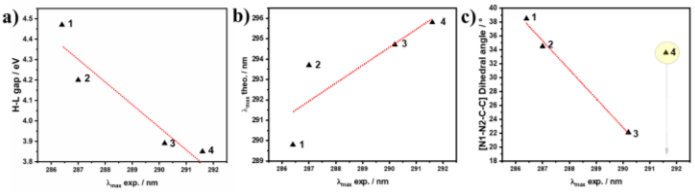

Figure 6. Experimental-theoretical correlations for compounds **1** – **4**.

The topological analysis based on the localized-orbital locator function (LOL-π) was performed to explore the above. The LOL-π function identifies electron π-delocalization in molecules by capturing the overlapping of localized orbitals due to an orbital gradient (see Supporting Information).[46,47] Figure 7 depicts the LOL-*π* surfaces for the out-of-plane *π*-conjugation (*xy*-plane) obtained for **1** – **4** and captures the conjugation between the N2-N3 sites of the triazole ring and the atoms of the R-group (note that the preferential electron delocalization path is more intense in the green to red zones). The higher *π*-bonding in **4** involving the extra phenyl ring in the phenyl-pyridine substituent is evidenced, causing a lower π-contribution of N2-N3 unit to the conjugation. Figure S15 represents the hole-electron surfaces for the electronic transition computed for **1** – **4** (that involves the HOMO, LUMO, and LUMO+1). This analysis allows us to corroborate the intramolecular CT (ICT) nature of the electronic transitions. It is observed that the transitions occur mainly from the methylthio-phenyl-C(4)-1,2,3-triazole moiety to the corresponding R-substituent. The ICT is favored for **2**, **3,** and **4** and less for **1** due to the electron-donating character of -OH. This explains the redshift of the λ_{max} and could be related to the absence of the shoulder in **1**, compared with **3** and **4**, and therefore, being contained in the λ_{max} adsorption band. This is also true for **2**, to which a low contribution of the iodine atom in the transitions is evidenced.

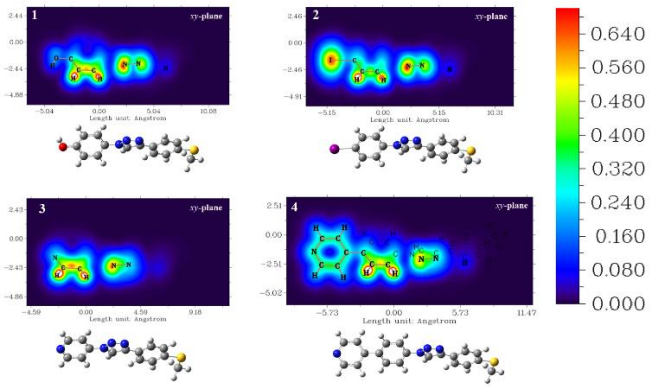

Figure 7. LOL-*π* surfaces plotted for the π-bonding orbitals of molecules **1** – **4** (1.2 Bohr distance on the *xy* plane).

CONCLUSIONS

In conclusion, the synthesis and characterization of the 1,2,3-triazoles substituted with aryl moieties were successfully performed. The synthesis involved the preparation of azide derivatives from the respective precursors, followed by a click reaction to obtain the target compounds. The overall yields were high, with over 75% yield for the azide derivatives and over 77% yield for the final compounds.

The characterization of the synthesized compounds was carried out using ^{1}H and ^{13}C NMR spectroscopy, as well as FT-IR spectroscopy. The NMR analysis provided insights into the chemical shifts of the different proton environments within the compounds. Distinctive signal patterns were observed in the ^{1}H NMR spectra, representing the triazole core, aromatic, and methyl groups. Compound **1** exhibited an additional signal corresponding to the OH group, which displayed a high-field shift. FT-IR spectroscopy confirmed the presence of the five-membered triazole ring, as evidenced by characteristic stretching frequencies. Compound **1** showed an additional stretching band corresponding to the O-H group.

The TD-DFT theoretical calculations explained the experimental UV-Vis properties of compounds **1** – **4**, revealing the occurrence of intramolecular charge transfer processes from the methylthio-phenyl-C(4)-1,2,3-triazole moiety to the corresponding R-substituent. The ICT is less favored for compound **1** due to the electron-donating -OH group, while it is more favored for compounds **2**, **3**, and **4**. The observed redshift of the λ_{max} band for **3** and **4** (as the appearance of the shoulders) is explained by the electron-withdrawing nature of the pyridine and phenyl-pyridine moieties, respectively. The additional phenyl ring in the R-substituent in **4** increases the electronic π-conjugation, thereby favoring the ICT process and leading to a higher redshift in its λ_{max} band compared with the other structures.

Overall, the synthesis and characterization results provide valuable information about the molecular structures and properties of the 1,2,3-triazoles substituted with aryl moieties analogs. These findings contribute to understanding their potential applications and pave the way for further investigations and utilization of these compounds in various fields, such as coordination chemistry and materials science.

CREDIT AUTHORSHIP CONTRIBUTION STATEMENT

Cristian Valdebenito: Formal analysis, Methodology. **David Moreno**: Formal analysis, Methodology, Writing, Investigation. **José Gaete:** Formal analysis, Investigation, Writing – review & editing. **Alejandro Toro-Labbé**: Conceptualization, Methodology, Writing – review & editing. **Karina Muñoz-Becerra**: Conceptualization, Methodology, Writing – review & editing. **Gabriel Abarca:** Funding acquisition, Resources, Writing- Reviewing and Editing. **Cesar Morales-Verdejo:** Funding acquisition, Resources, Supervision, Writing-Original draft preparation, Reviewing and Editing.

DECLARATION OF COMPETING INTERESTS

The authors declare that they have no known competing financial interests or personal relationships that could have appeared to influence the work reported in this paper.

SUPPORTING INFORMATION

NMR, FT-IR, UV-vis and Theoretical Calculations for all compounds related to this article can be found in supplementary data.

ACKNOWLEDGMENTS

We gratefully acknowledge the financial support of FONDECYT projects 11221073, 1210827, 1230991, and ANILLO project ACT-192175.

REFERENCES

1. Dixit, D.; Verma, P. K.; Marwaha, R. K. A Review on 'Triazoles': Their Chemistry, Synthesis and Pharmacological Potentials. *Journal of the Iranian Chemical Society* **2021**, *18* (10), 2535–2565. https://doi.org/10.1007/s13738-021-02231-x.
2. Hua, Y.; Flood, A. H. Click Chemistry Generates Privileged CH Hydrogen-Bonding Triazoles: The Latest Addition to Anion Supramolecular Chemistry. *Chem Soc Rev* **2010**, *39* (4), 1262. https://doi.org/10.1039/b818033b.
3. Hein, J. E.; Fokin, V. V. Copper-Catalyzed Azide–Alkyne Cycloaddition (CuAAC) and beyond: New Reactivity of Copper(i) Acetylides. *Chem Soc Rev* **2010**, *39* (4), 1302. https://doi.org/10.1039/b904091a.
4. Neto, J. S. S.; Zeni, G. A Decade of Advances in the Reaction of Nitrogen Sources and Alkynes for the Synthesis of Triazoles. *Coord Chem Rev* **2020**, *409*, 213217. https://doi.org/10.1016/j.ccr.2020.213217.
5. Mustafa, M.; Abdelhamid, D.; Abdelhafez, E. M. N.; Ibrahim, M. A. A.; Gamal-Eldeen, A. M.; Aly, O. M. Synthesis, Antiproliferative, Anti-Tubulin Activity, and Docking Study of New 1,2,4-Triazoles as Potential Combretastatin Analogues. *Eur J Med Chem* **2017**, *141*, 293–305. https://doi.org/10.1016/j.ejmech.2017.09.063.
6. Dehestani, L.; Ahangar, N.; Hashemi, S. M.; Irannejad, H.; Honarchian Masihi, P.; Shakiba, A.; Emami, S. Design, Synthesis, in Vivo and in Silico Evaluation of Phenacyl Triazole Hydrazones as New Anticonvulsant Agents. *Bioorg Chem* **2018**, *78*, 119–129. https://doi.org/10.1016/j.bioorg.2018.03.001.
7. Kaushik, C. P.; Pahwa, A. Convenient Synthesis, Antimalarial and Antimicrobial Potential of Thioethereal 1,4-Disubstituted 1,2,3-Triazoles with Ester Functionality. *Medicinal Chemistry Research* **2018**, *27* (2), 458–469. https://doi.org/10.1007/s00044-017-2072-x.
8. Al-Masoudi, N. A.; Al-Soud, Y. A. Synthesis of 1′-β-d-Glucopyranosyl-1,2,3-Triazole-4,5-Dimethanol-4,5-Bis(Isopropylcarbamate) as Potential Antineoplastic Agent. *Tetrahedron Lett* **2002**, *43* (22), 4021–4022. https://doi.org/10.1016/S0040-4039(02)00733-5.
9. Cao, X.; Wang, W.; Wang, S.; Bao, L. Asymmetric Synthesis of Novel Triazole Derivatives and Their in Vitro Antiviral Activity and Mechanism of Action. *Eur J Med Chem* **2017**, *139*, 718–725. https://doi.org/10.1016/j.ejmech.2017.08.057.
10. Sarigol, D.; Uzgoren-Baran, A.; Tel, B. C.; Somuncuoglu, E. I.; Kazkayasi, I.; Ozadali-Sari, K.; Unsal-Tan, O.; Okay, G.; Ertan, M.; Tozkoparan, B. Novel Thiazolo[3,2-b]-1,2,4-Triazoles Derived from Naproxen with Analgesic/Anti-Inflammatory Properties: Synthesis, Biological Evaluation and Molecular Modeling Studies. *Bioorg Med Chem* **2015**, *23* (10), 2518–2528. https://doi.org/10.1016/j.bmc.2015.03.049.
11. Tantray, M. A.; Khan, I.; Hamid, H.; Alam, M. S.; Umar, S.; Ali, Y.; Sharma, K.; Hussain, F. Synthesis of Novel Oxazolo[4,5-b]Pyridine-2-One Based 1,2,3-Triazoles as Glycogen Synthase Kinase-3 β Inhibitors with Anti-Inflammatory Potential. *Chem Biol Drug Des* **2016**, *87* (6), 918–926. https://doi.org/10.1111/cbdd.12724.
12. Safavi, M.; Ashtari, A.; Khalili, F.; Mirfazli, S. S.; Saeedi, M.; Ardestani, S. K.; Rashidi Ranjbar, P.; Barazandeh Tehrani, M.; Larijani, B.; Mahdavi, M. Novel Quinazolin-4(3 H)-One Linked to 1,2,3-Triazoles: Synthesis and Anticancer Activity. *Chem Biol Drug Des* **2018**, *92* (1), 1373–1381. https://doi.org/10.1111/cbdd.13203.
13. Thakkar, S. S.; Thakor, P.; Doshi, H.; Ray, A. 1,2,4-Triazole and 1,3,4-Oxadiazole Analogues: Synthesis, MO Studies, in Silico Molecular Docking Studies, Antimalarial as DHFR Inhibitor and Antimicrobial Activities. *Bioorg Med Chem* **2017**, *25* (15), 4064–4075. https://doi.org/10.1016/j.bmc.2017.05.054.
14. Nadeem, M.; Yunus, U.; Bhatti, M. H.; Ayub, K.; Mehmood, M.; Saif, M. J. Crystal Structure, Spectroscopic, Electronic, Luminescent and Nonlinear Optical Properties of (S)-4-Amino-5-(1-Hydroxy-Ethyl)-2,4-Dihydro-[1,2,4]Triazole-3-Thione: A Combined Experimental and DFT Study. *Journal of Physics and Chemistry of Solids* **2017**, *110*, 218–226. https://doi.org/10.1016/j.jpcs.2017.06.011.
15. Hempel, C.; Maichle-Mössmer, C.; Pericàs, M. A.; Nachtsheim, B. J. Modular Synthesis of Triazole-Based Chiral Iodoarenes for Enantioselective Spirocyclizations. *Adv Synth Catal* **2017**, *359* (17), 2931–2941. https://doi.org/10.1002/adsc.201700246.
16. Rossi, R.; Bellina, F.; Lessi, M.; Manzini, C.; Perego, L. Synthesis of Multiply Arylated Heteroarenes, Including Bioactive Derivatives, via Palladium-Catalyzed Direct C–H Arylation of Heteroarenes with (Pseudo)Aryl Halides or Aryliodonium Salts. *Synthesis (Stuttg)* **2014**, *46* (21), 2833–2883. https://doi.org/10.1055/s-0034-1378674.
17. Haldón, E.; Nicasio, M. C.; Pérez, P. J. Copper-Catalysed Azide–Alkyne Cycloadditions (CuAAC): An Update. *Org Biomol Chem* **2015**, *13* (37), 9528–9550. https://doi.org/10.1039/C5OB01457C.
18. Kolb, H. C.; Sharpless, K. B. The Growing Impact of Click Chemistry on Drug Discovery. *Drug Discov Today* **2003**, *8* (24), 1128–1137. https://doi.org/10.1016/S1359-6446(03)02933-7.
19. Pizarro, A.; Abarca, G.; Gutiérrez-Cerón, C.; Cortés-Arriagada, D.; Bernardi, F.; Berrios, C.; Silva, J. F.; Rezende, M. C.; Zagal, J. H.; Oñate, R.; Ponce, I.

Building Pyridinium Molecular Wires as Axial Ligands for Tuning the Electrocatalytic Activity of Iron Phthalocyanines for the Oxygen Reduction Reaction. *ACS Catal* **2018**, *8* (9), 8406–8419. https://doi.org/10.1021/acscatal.8b01479.

20. Fan, Y.; Pitie, S.; Liu, C.; Zhao, C.; Zhao, C.; Seydou, M.; Dappe, Y. J.; Nichols, R. J.; Yang, L. Asymmetric Effect on the Length Dependence of Oligo(Phenylene Ethynylene)-Based Molecular Junctions. *The Journal of Physical Chemistry C* **2022**, *126* (7), 3635–3645. https://doi.org/10.1021/acs.jpcc.1c07654.
21. Gunderson, V. L.; Smeigh, A. L.; Kim, C. H.; Co, D. T.; Wasielewski, M. R. Electron Transfer within Self-Assembling Cyclic Tetramers Using Chlorophyll-Based Donor–Acceptor Building Blocks. *J Am Chem Soc* **2012**, *134* (9), 4363–4372. https://doi.org/10.1021/ja211329k.
22. M. J. Frisch, G. W. Trucks, H. B. Schlegel, G. E. Scuseria, M. A. Robb, J. R. Cheeseman, G. Scalmani, V. Barone, G. A. Petersson, H. Nakatsuji, M. C. X. Li, A. Marenich, J. Bloino, B. G. Janesko, R. Gomperts, B. Mennucci, H. P. Hratchian, J. V. Ortiz, A., D. J. F. Gaussian 16, Revision C.01, Gaussian, Inc., Wallingford CT, 2016.
Defined by the Bulk Dielectric Constant and Atomic Surface Tensions. *J Phys Chem B* **2009**, *113* (18), 6378–6396. https://doi.org/10.1021/jp810292n.
28. Chiodo, S.; Russo, N.; Sicilia, E. LANL2DZ Basis Sets Recontracted in the Framework of Density Functional Theory. *J Chem Phys* **2006**, *125* (10). https://doi.org/10.1063/1.2345197.
29. An, S.; Meng, S.; Xue, J.; Wang, H.; Zheng, X.; Zhao, Y. UV–Vis, Raman Spectroscopic and Density Functional Theoretical Studies on Microsolvation 1, 2, 4-Triazole-3-Thione Clusters. *Spectrochim Acta A Mol Biomol Spectrosc* **2021**, *258*, 119762. https://doi.org/10.1016/j.saa.2021.119762.
30. Tankov, I.; Yankova, R. Hirshfeld Surface, DFT Vibrational (FT-IR) and Electronic (UV–Vis) Studies on 4-Amino-1H-1,2,4-Triazolium Nitrate. *J Mol Struct* **2019**, *1179*, 581–592. https://doi.org/10.1016/j.molstruc.2018.11.050.
31. Gökalp, M.; Dede, B.; Tilki, T.; Karabacak Atay, Ç. Triazole Based Azo Molecules as Potential Antibacterial Agents: Synthesis, Characterization, DFT, ADME and Molecular Docking Studies. *J Mol Struct* **2020**, *1212*, 128140. https://doi.org/10.1016/j.molstruc.2020.128140.
32. Zych, D.; Slodek, A. The Impact of a 1,2,3-Triazole Motif on the Photophysical Behavior of Non-K Tetrasubstituted Pyrene with a Substitution Pattern Providing the Long Axial Symmetry. *Molecules* **2022**, *27* (13), 4314. https://doi.org/10.3390/molecules27134314.
33. Padalkar, V. S.; Lanke, S. K.; Chemate, S. B.; Sekar, N. N-2-Aryl-1,2,3-Triazoles: A Novel Class of Blue Emitting Fluorophores-Synthesis, Photophysical Properties Study and DFT Computations. *J Fluoresc* **2015**, *25* (4), 985–996. https://doi.org/10.1007/s10895-015-1580-7.
34. Wang, T.-H.; Chu, H.-Y.; Wang, I.-T. Structures, Molecular Orbitals and UV–Vis Spectra Investigations on Methyl 1-Benzyl-1H-1,2,3-Triazole-4-Carboxylate: A Computational Study. *Spectrochim Acta A Mol Biomol Spectrosc* **2014**, *131*, 268–273. https://doi.org/10.1016/j.saa.2014.04.133.
35. Kim, T. Y.; Elliott, A. B. S.; Shaffer, K. J.; John McAdam, C.; Gordon, K. C.; Crowley, J. D. Rhenium(I) Complexes of Readily Functionalized Bidentate Pyridyl-1,2,3-Triazole "Click" Ligands: A Systematic Synthetic, Spectroscopic and Computational Study. *Polyhedron* **2013**, *52*, 1391–1398. https://doi.org/10.1016/j.poly.2012.05.003.
36. Tamer, Ö.; Bhatti, M. H.; Yunus, U.; Nadeem, M.; Avcı, D.; Atalay, Y.; Yaqub, A.; Quershi, R. Structure-Property Relationship of 3-(N-Phthalimidomethyl)-4-Amino-1,2,4-Triazole-5-Thione: A Structural, Spectroscopic and DFT Study. *J Mol Struct* **2017**, *1133*, 329–337. https://doi.org/10.1016/j.molstruc.2016.12.017.
37. Grimme, S.; Ehrlich, S.; Goerigk, L. Effect of the Damping Function in Dispersion Corrected Density Functional Theory. *J Comput Chem* **2011**, *32* (7), 1456–1465. https://doi.org/10.1002/jcc.21759.
38. Lu, T.; Chen, F. Multiwfn: A Multifunctional Wavefunction Analyzer. *J Comput Chem* **2012**, *33* (5), 580–592. https://doi.org/10.1002/jcc.22885.
39. Rukmanikrishnan, B.; Muthusamy, S. Preparation and Properties of Polyimides Containing 1,2,3-Triazole Moieties. *Advances in Polymer Technology* **2018**, *37* (1), 50–59. https://doi.org/10.1002/adv.21641.
40. Gavlik, K. D.; Sukhorukova, E. S.; Shafran, Y. M.; Slepukhin, P. A.; Benassi, E.; Belskaya, N. P. 2-Aryl-5-Amino-1,2,3-Triazoles: New Effective Blue-Emitting Fluorophores. *Dyes and Pigments* **2017**, *136*, 229–242. https://doi.org/10.1016/j.dyepig.2016.08.015.
41. Săcărescu, L.; Dascălu, M.; Chibac-Scutaru, A.-L.; Roman, G. Synthesis, Structural Characterization, Photophysical Study and Investigation as Fluorescent Sensor towards Metal Ions of 1,2,3-Triazole–Azaindene Hybrids. *J Photochem Photobiol A Chem* **2022**, *433*, 114160. https://doi.org/10.1016/j.jphotochem.2022.114160.
23. Stephens, P. J.; Devlin, F. J.; Chabalowski, C. F.; Frisch, M. J. Ab Initio Calculation of Vibrational Absorption and Circular Dichroism Spectra Using Density Functional Force Fields. *J Phys Chem* **1994**, *98* (45), 11623–11627. https://doi.org/10.1021/j100096a001.
24. Kim, K.; Jordan, K. D. Comparison of Density Functional and MP2 Calculations on the Water Monomer and Dimer. *J Phys Chem* **1994**, *98* (40), 10089–10094. https://doi.org/10.1021/j100091a024.
25. Lee, C.; Yang, W.; Parr, R. G. Development of the Colle-Salvetti Correlation-Energy Formula into a Functional of the Electron Density. *Phys Rev B* **1988**, *37* (2), 785–789. https://doi.org/10.1103/PhysRevB.37.785.
26. Hehre, W. J.; Pau, C. Fong.; Headley, A. D.; Taft, R. W.; Topsom, R. D. A Scale of Directional Substituent Polarizability Parameters from Ab Initio Calculations of Polarizability Potentials. *J Am Chem Soc* **1986**, *108* (7), 1711–1712. https://doi.org/10.1021/ja00267a063.
27. Marenich, A. V.; Cramer, C. J.; Truhlar, D. G. Universal Solvation Model Based on Solute Electron Density and on a Continuum Model of the Solvent
42. Yan, W.; Wang, Q.; Lin, Q.; Li, M.; Petersen, J. L.; Shi, X. N-2-Aryl-1,2,3-Triazoles: A Novel Class of UV/Blue-Light-Emitting Fluorophores with Tunable Optical Properties. *Chemistry - A European Journal* **2011**, *17* (18), 5011–5018. https://doi.org/10.1002/chem.201002937.
43. Laird, R. C.; Nguyen, N. P.; Rusch, S. F.; Baltrusaitis, J.; MacGillivray, L. R. Noncentrosymmetric Packings Influenced by Electronic Properties of Products of Click Reactions. *Cryst Growth Des* **2014**, *14* (3), 893–896. https://doi.org/10.1021/cg4016542.
44. Singh, H.; Sindhu, J.; Khurana, J. M. Synthesis and Photophysical Properties of Novel Chloroquinoline Based Chalcone Derivates Containing 1,2,3-Triazole Moiety. *J Lumin* **2015**, *158*, 340–350. https://doi.org/10.1016/j.jlumin.2014.10.047.
45. Che, Y.; Perepichka, D. F. Quantifying Planarity in the Design of Organic Electronic Materials. *Angewandte Chemie International Edition* **2021**, *60* (3), 1364–1373. https://doi.org/10.1002/anie.202011521.
46. Cheng, X.; Zhang, X.; Zhao, Y.; Zhuo, L. Theoretical Investigation of the Borazine B9N9 Monocyclic Ring. *Chem Phys Lett* **2023**, *821*, 140476. https://doi.org/10.1016/j.cplett.2023.140476.
47. Steinmann, S. N.; Mo, Y.; Corminboeuf, C. How Do Electron Localization Functions Describe π-Electron Delocalization? *Physical Chemistry Chemical Physics* **2011**, *13* (46), 20584. https://doi.org/10.1039/c1cp21055f.